Transpiration Cooling With Liquid Metals

A. T. Robinson,* R. L. McAlexander,† J. D. Ramsdell,* and M. R. Wolfson*
U. S. Naval Ordnance Test Station, China Lake, Calif.

The development of hybrid propulsion concepts at the Naval Ordnance Test Station has created the requirement for a lightweight nozzle system capable of withstanding gas temperatures in excess of 6200°F for burn times longer than 30 sec. A series of 40 nozzle-material test firings illustrated that tungsten nozzle insert systems provided the best operation. The inserts tested included tungsten metal-oxide compacts and tungsten infiltrated with metals selected on the basis of their latent heats of vaporization and boiling points. Temperature-time profiles taken during firings indicated that heat transfer rates were lower with the tungsten-metal systems than for unmodified tungsten, which indicated the possibility that transpiration or mass transfer cooling was being realized. A laboratory program was initiated to subject infiltrated tungsten samples to a plasma-arc heat source. It was found that, during exposure to high heat fluxes, temperatures were reduced by inducing flow of the molten infiltrant by pressurizing the back side of the specimen. This technique, in combination with ablative sacrificial materials, offers an excellent nozzle system for long-time firing durations in hybrid and solid propellant rockets.

Introduction

A CONSIDERABLE portion of present-day materials technological effort is being expended on system development to survive high temperature environment. Current use of high energy propellants subjects the hot gas side of rocket motor nozzles to heat fluxes ranging from 15 to 35 Btu/in.^{2}/sec. Leading edges of lift re-entry vehicles are exposed to less severe environments for longer periods of time. The general approaches to combat this high temperature problem fall within the disciplines of the following categories: transpiration, ablation, radiation, and convective cooling with and without an additional heat sink structure. However, the weight or volume penalties, in addition to design considerations, complicate their use in a workable flight model.

The Naval Ordnance Test Station has experimented with several of the foregoing concepts for nozzle cooling in a static test motor. The system that has demonstrated the best possibilities to date has been a combination of ablation and transpiration cooling. Ablation cooling was achieved through the use of sacrificial materials placed forward of the nozzle, and transpiration cooling was provided by the mass flow of liquid metals through a porous tungsten insert. Results of ablation cooling experiments were previously reported,[1] and so this paper deals primarily with materials evaluation and transpiration cooling by liquid metals.

Hybrid Static Motor Tests

Materials testing was performed with a 12-in.-diam static hybrid motor mounted horizontally (Fig. 1). The firing bay contained complete instrumentation facilities for recording motor performance and nozzle temperature at several locations.

A majority of tests were made with metallized polyurethane propellants as the solid portion of the propellant system. Inhibited red fuming nitric acid was injected during firing, giving a theroretical flame temperature of 6200°F at 1000 psi pressure.

The nozzles used for most of the tests had a $1\frac{1}{2}$-in.-diam throat. Some of the later firings used a 1.430-in. throat for higher chamber pressures. Thermocouples were placed at various depths and positions so that the time-temperature information obtained could be used for subsequent thermal analysis. Several types of thermocouple were used, depending upon the expected temperature rise. In all cases, they were electrically insulated in magnesium oxide or other ceramic and sheathed with stainless steel or tantalum. It was found that C-6 graphite cement was a suitable potting compound for holding the thermocouple sheaths to the wall of the graphite housing. Fig. 2 indicates the general features of the test nozzle and indicates a typical arrangement of thermocouple positions.

The first tests were performed primarily to evaluate a series of representative refractory materials that could be used as a throat insert in an uncooled hot-structure design. Graphite was selected as a holder on the basis of weight and thermal heat capacity. The materials that gave the best performance for a firing time of 8 sec were duplicated for 16-sec firings. Fig. 3 indicates the relative merit in their ability to resist erosion. After firing, each insert was measured for erosion and sectioned for metallographic analysis.

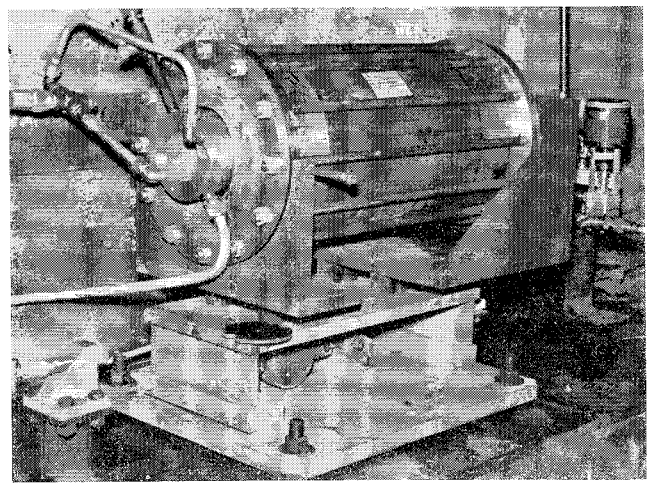

Fig. 1 12-in. hybrid motor on static test stand (official U. S. Navy photograph)

Presented at the ARS Launch Vehicles: Structures and Materials Conference, Phoenix, Ariz., April 3–5, 1962; revision received November 2, 1962.

* Metallurgist. Member ARS.

† Aerospace Power Engineer. Member ARS.

[1] McAlexander, R. L., Donaldson, W. E., and Robinson, A. T., "Comparison of heat transfer and erosion rates from nozzle firings with and without sacrificial barrier," ARS J. **32**, 1276–1278 (1962).

Table 1 Description of hybrid nozzle material evaluation tests

Firing no.	Nozzle no.	Insert material	Holder/adapter back-up material	Additional cooling	Ablative shield	Injection time, sec	Erosion % area increase	Remarks
LC-203	1	Graphite	None	None	None	<1.0	...	Oxidizer lines blew out in 0.7 sec.
LC-204	2	Graphite	None	None	None	8	30	Injector eroded, poor mixing.
LC-205	3	90 tantalum-10 tungsten	Graphite	None	None	8	64.0	Insert ejected in 7.5 sec, nonuniform erosion.
LC-206	4	85 tungsten-15 molybdenum	Graphite	None	None	8	0	Injector eroded.
LC-207	5	Spun tantalum, 0.040 in. thick	Graphite	None	None	8	44.0	Insert ejected 0.4 sec after ignition.
LC-208	6	Spun tungsten, 0.040 in. thick	Graphite	None	None	8	36.0	Insert ejected 2.5 sec after ignition.
LC-219	7	Tungsten, copper impregnated	Graphite	None	None	8	−7.5	1st time S-S injector used.
LC-220	8	Tungsten-Al_2O_3 compact	Graphite	None	None	8	−2.0	High chamber pressure restricted flow of oxidizer.
LC-221	9	Zirconia phenolic reinforced oxide fibers	Graphite	None	None	8	108	Drop in pressure indicates gradual and complete erosion with time.
LC-222	10	Tungsten-BeO compact	Graphite	None	None	8	0	Insert fragmented.
LC-223	11	Tungsten-BeO compact	Graphite	None	None	16	...	Insert ejected.
LC-224	12	Laminated tungsten-phenolic zirconia fiber reinforced	Graphite	None	None	16	170	Complete erosion gradual.
LC-241	13	Graphite (CVD)	Graphite	Water	None	24.25	183	Ballistic data on C-1000 propellant.
LC-242	14	Tungsten, Cu impregnated	Graphite	None	None	18	5.1	Successful operation but motor performance low.
LC-243	15	Graphite cloth phenolic	Graphite	None	None	8	14.0	Motor performance low.
LC-244	16	Tungsten-Al_2O_3 compact	Graphite	None	None	18	10.3	Oxidizer flow restricted.
LC-245	17	Stainless steel	Graphite	Film (H_2O) cooled	None	8	57.5	Complete erosion-nozzle may have lasted for 2 sec.
LC-246	18	85 tungsten-15 molybdenum	Molybdenum	Water	W-Cu	18	3.6	Satisfactory performance.
LC-259	19	90 tantalum-10 tungsten	Graphite	Graphite	Graphite cloth-phenolic	8	−11.0	High chamber pressure resulting in low L/S ratio.
LC-260	20	Spun molybdenum, 0.040 in. thick	Graphite	None	None	8	30.0	Insert ejected in 4.5 sec.
LC-261	21	Tungsten (P and S)	Graphite					Motor malfunctioned at 3.7 sec, insert refired on no. 36.
LC-278	22	Tungsten, brass impregnated	Graphite	None	None	18	42	Erosion in W-brass more severe than with W-Cu.
LC-279	23	Tungsten (P and S), 90% density	Graphite	None	None	18	18	Erosion greater than with W-Cu.
LC-280	24	Graphite cloth-phenolic	Graphite	None	Graphite cloth-phenolic	8	29	More erosion than in previous test with graphite-cloth.
LC-281	25	XP 202 cloth	Graphite	None	None	8	96	Erosion greater than plain graphite.
LC-282	26	Graphite (CVD)	Graphite	H_2O	None	7.2	58	Reignition occurred about 30 to 40 sec after water quench.
LC-283	27	Tungsten, Cu impregnated, 81% density	Graphite	None	Graphite cloth-phenolic	18	6	Injector failed restricting oxidizer flow.
LC-297	28	Tungsten, Cu impregnated, 81% density	Graphite	None	Graphite cloth-phenolic	18	1.7	Slight erosion in insert where ablative shield eroded.
LC-298	29	Tungsten, Cu impregnated, 73% density	Graphite	H_2O	Graphite cloth-phenolic	15	90	Uneven erosion, contoured nozzle.
LC-299	30	Tungsten, Cu impregnated, 73% density	Graphite	H_2O	Graphite cloth-phenolic	15	71.5	Uneven erosion, contoured nozzle.
LC-300	31	Tungsten, Cu impregnated, 73% density	Graphite	H_2O	Graphite cloth-phenolic	1.2	...	Nozzle plugged after 0.5 sec by igniter.
LC-301	32	Tungsten, Cu impregnated, 77% density	Molybdenum	H_2O	Graphite cloth-phenolic	25	38	Uniform erosion.
LC-302	33	Tungsten, Cu impregnated, 77% density	Molybdenum	H_2O	Graphite cloth-phenolic	25	55	Gouges in insert where ablative shield eroded.
LC-315	34	Tungsten, Cu impregnated, 73% density	Graphite	H_2O	Graphite cloth-phenolic	15	18	Fairly uniform erosion, contoured nozzle.
LC-316	35	Tungsten, Cu impregnated, 65% density	Graphite	None	None	18	122	Insert ejected after 11.8 sec.

Table 1 (Continued)

Firing no.	Nozzle no.	Insert material	Holder/adapter back-up material	Additional cooling	Ablative shield	Injection time, sec	Erosion % area increase	Remarks
LC-317	36	Tungsten, 90% density	Coated graphite, 0.003 Ta, 0.012 ThO + H_2O	None	None	18	11.0	Refired insert no. 21, some pitting, improvement over no. 23.
LC-318	37	Tungsten, Cu impregnated, 84.5% density	Molybdenum	H_2O	Graphite cloth-phenolic	25	258	Half of insert and part of molybdenum holder eroded away.
LB-996	39	Tungsten, Cu impregnated, 80% density	Molybdenum	H_2O	Graphite cloth-phenolic	30	18	Nozzle insert blew out, some erosion of holder.
RS-6384	40	Tungsten, Cu impregnated	Graphite	None	Graphite cloth-phenolic	16	4.32	Satisfactory performance.

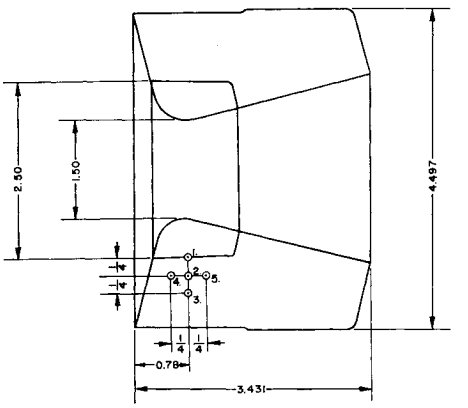

Fig. 2 Nozzle section

The more promising materials from the first group of tests were redesigned into other nozzle configurations that incorporated some type of cooling mechanism. These tests were also instrumented for temperature measurements to provide a comparison with the previous firings. Insert geometry and size were duplicated whenever possible. Identification of the test firings is contained in Table 1.

Evaluation Based on Hybrid Tests

Data obtained from the firings showed that the nozzles of the hot-structure concept experienced excessive erosion in 18 sec. If higher performance propellants or longer firing times are to be used, then some method must be used to reduce the steady-state hot-wall temperature. A trend was noted from the foregoing tests: inserts of different basic refractories permitted about the same degree of temperature rise in the graphite heat sink material. Attention is called to Fig. 4, which shows the time-temperature history at the insert-graphite interface of a tungsten insert infiltrated with copper and that of a pressed and sintered tungsten-beryllium oxide insert.‡ The interfacial temperatures are almost identical through the complete firing. The lower curves, which indicate the temperature $\frac{1}{4}$ in. below the insert holder, are also very nearly the same. These equal temperature gradients reveal that the quantity of heat passing through each insert is the same. Additional evidence of this trend is shown again in Fig. 5. Here, data from a series of different refractory inserts, which were tested under the same conditions, are shown. The curves show that the insert-graphite holder interface in all tests experienced about the same temperature-time history. A spread of approximately 400°F persists between the highest and lowest interface temperatures for the complete duration. Examination of inserts after firing indicates that this difference is not sufficient to produce a marked decrease in erosion. The lowest curves were obtained with tungsten infiltrated with copper and the tungsten-beryllium oxide compact. It was suspected that these two materials may have benefited by transpiration cooling. Metallographic analysis confirmed that copper did migrate to the surface; however, the depth of removal was only a few millimeters, and the major portion remained within the insert.

Fig. 6 indicates the improvement that can be achieved through the addition of a flowing-water coolant surrounding the heat sink holder. The continuous removal of heat by the water coolant approaches the conditions of an infinite heat sink. A cylinder of tungsten infiltrated with copper was placed just forward of the 85 tungsten-15 molybdenum insert. This was put in to decrease impact of the combustion gases in the forward part of the throat and help channel the

‡ The tungsten-copper insert was a sintered compact before infiltration; the tungsten-beryllium oxide was pressed and sintered mixed powders.

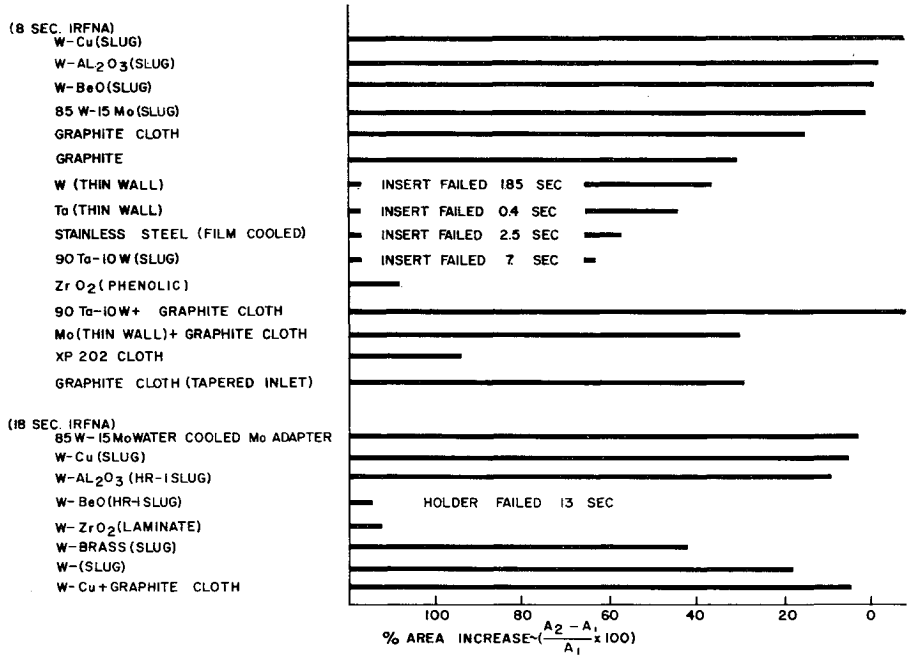

Fig. 3 Erosion of various nozzle materials used in hybrid firings (official U. S. Navy photograph)

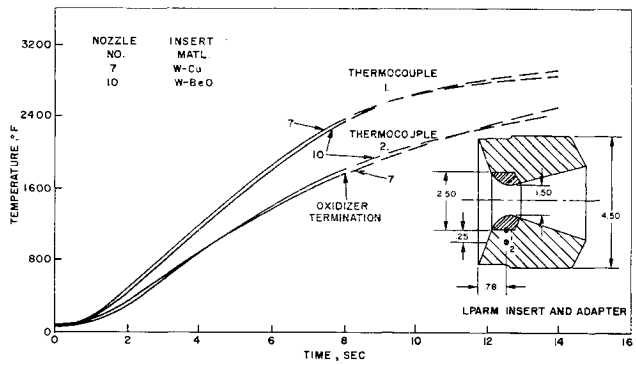

Fig. 4 Nozzle temperature-time data for tungsten infiltrated with copper and tungsten-beryllium oxide inserts

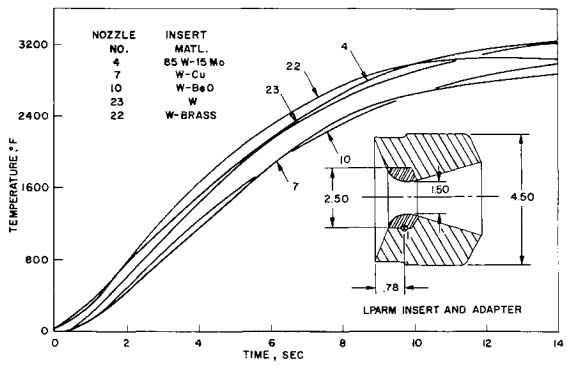

Fig. 5 Nozzle temperature-time data for various insert materials

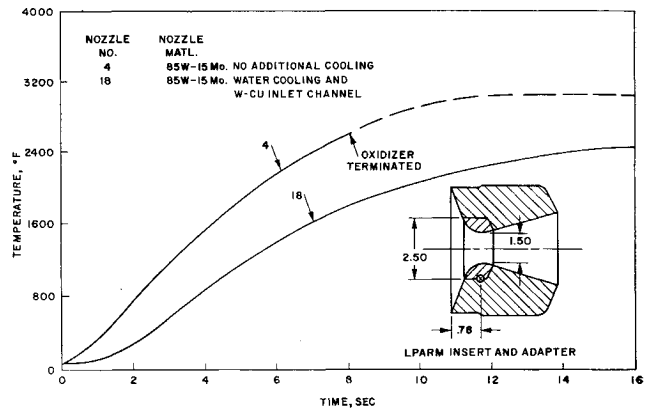

Fig. 6 Nozzle temperature-time data for 85W-15 Mo insert with and without water cooling and W-Cu inlet channel

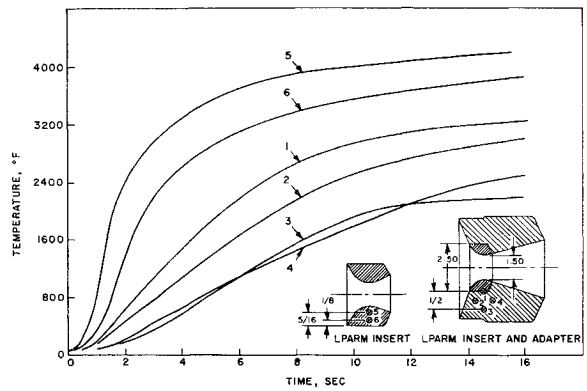

Fig. 7 Temperature-time data for tungsten insert-graphite holder

gas flow. A calculation based on the temperature measurements during firing reveals that the hot wall temperature has been reduced from 4600° to 4200°F. Nozzle erosion was reduced to just 3.6% area increase, permitting successful operation of the motor for a period of 18 sec.

The time-temperature curves of Fig. 7 were taken from thermocouples located at various positions in a tungsten insert and graphite holder. The relatively high temperatures from the thermocouple at position 2, as compared to the thermocouple at position 4 and located at the same radius, reveal that considerable heat is being transferred into the nozzle through its frontal area. This additional heat input increases the structure temperature at a faster rate than would be anticipated under conditions of unidimensional heat flow and thereby lowers the efficiency by which it may absorb the heat from the tungsten insert.

Fig. 8 shows comparative temperatures that were obtained at the insert-holder interface for two nozzle geometries. By modifying the nozzle to a more gradual taper at the throat, the rate of temperature rise in the graphite has been reduced. It is believed that the longer insert with increased interfacial area provides a more efficient path for heat flow into the backup material.

Another method used effectively to decrease erosion has been the use of an ablative heat shield. Fig. 9 shows the

Table 2 Physical and thermal properties of various metals[a]

Element	Atomic weight	Melting point, °C	Boiling point, °C	ΔH_f, cal/g	ρ, g/cm³	ΔH_v, cal/g	ΔH_v, cal/cm³	C_p, cal/g/°C
Al	26.97	660	2450	94.5	2.699	2,520	6,790	0.215
Bi	209.00	271	1560	12.5	9.8	204.3	2,003	0.0294
Ce	140.13	804	3470	8.5	6.77	662	4,480	0.045
Co	58.94	1495	2900	58.4	8.85	1,500	13,290	0.099
Cu	63.57	1083	2595	50.6	8.96	1,272	11,400	0.092
Pb	207.21	327	1725	6.26	11.36	223	2,530	0.0309
Li	6.94	181	1330	104.2	0.534	4,638	2,466	0.79
Mg	24.32	650	1107	88	1.74	1,260	2,190	0.245
Mn	54.94	1245	2150	63.7	7.43	978	7,260	0.115
Hg	200.61	−38	357	2.8	13.546	69.7	944	0.033
Mo	95.95	2610	5560	69.8[b]	10.22	1,225	12,520	0.066
Si	28.66	1410	2680	432	2.33	2,535	5,900	0.162
Ag	107.88	961	2210	25	10.49	556	5,840	0.0559
Sn	118.70	232	2270	14.5	7.2984	570	4,150	0.054
W	183.92	3410	5930	44	19.3	1,150	22,200	0.033
Zn	65.38	420	906	24.1	7.133	425.6	3,040	0.0915

[a] Values obtained from *A.S.M. Metals Handbook*, 8th ed., Vol. 1, 1961, and *A.E.C. Reactor Handbook*, Vol. 3, March 1955.
[b] Estimated.

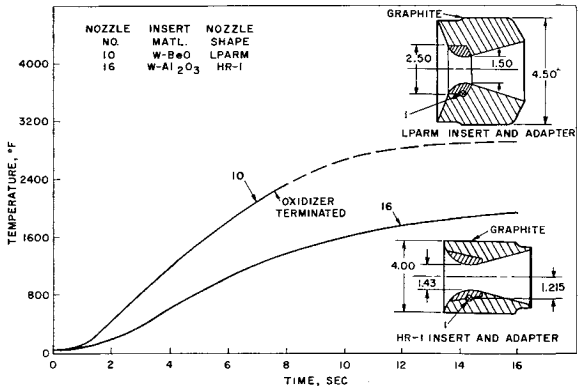

Fig. 8 Nozzle temperature-time data for two insert geometries

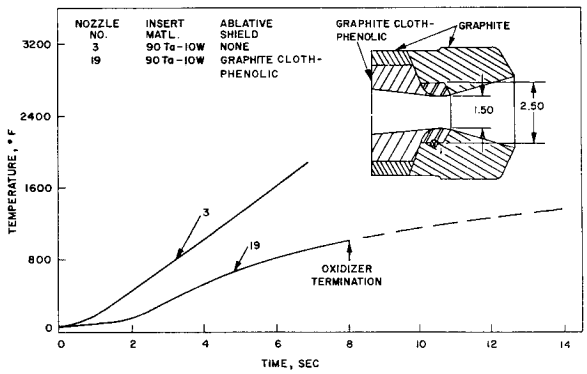

Fig. 9 Nozzle temperature-time data with and without graphite cloth ablative shield

decrease in the insert-holder interfacial temperature which was achieved by the use of a molded graphite cloth-phenolic block immediately in front of the insert. The block was shaped to protect the entrance section and help channel the gas stream. Its cooling effect is considered to be due largely to its ability to produce a cooler gas along the surface wall through decomposition of the plastic. Protection is also derived by the block acting as a barrier to the flow of heat into the face of the nozzle.

Based upon the material and design information obtained from these tests, five nozzles were fabricated for a 12-in. hybrid motor (see Fig. 10). They contained an insert of tungsten infiltrated with copper and had an entrance taper of a 10° half angle. A graphite cloth-phenolic ablation block was placed in front of the insert, and a $\frac{1}{4}$-in. sheet of phenolic

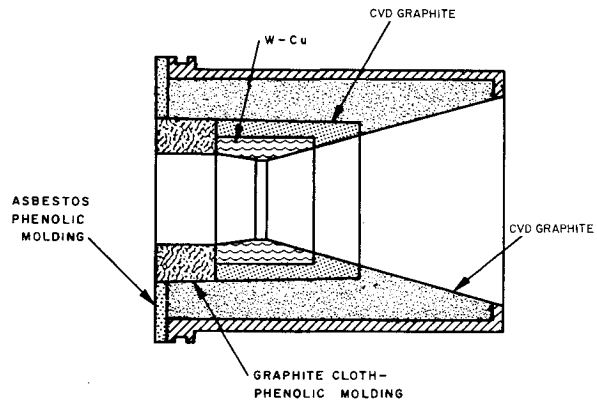

Fig. 10 Flightweight static test nozzle for 12-in. hybrid motor

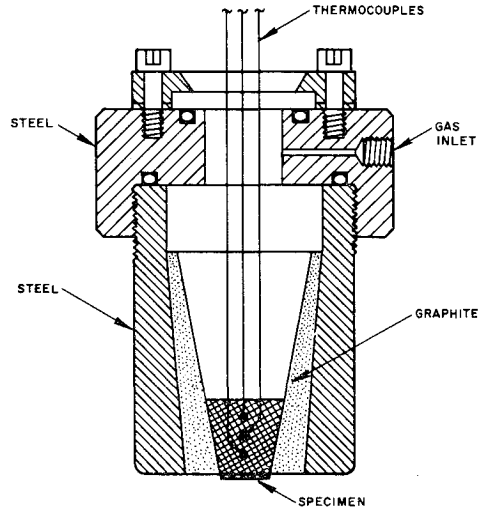

Fig. 11 Test fixture for plasma-jet transpiration cooling evaluation studies

asbestos was located in front of the ablation shield to act as a heat shield and to isolate the high temperature region. Three nozzles were fired statically for 18-sec durations with less than 5% area increase at the nozzle throat. Two successful flight tests were also made; erosion values were not available due to breakup on impact.

A preliminary investigation was made to determine heat transfer coefficients through a curve-fitting process using a two-layer, linear, one-space variable temperature time-dependent analysis. Curve fittings were performed on an

IBM 709 computer, and the heat transfer coefficient values were compared to those obtained from the Bartz equation. The results from the curve-fitting process resulted in heat transfer values lower by an order of magnitude than either predicted values or values obtained by the modified pipe flow equation. Because of the present difficulties encountered in setting up a mathematical model that takes into account the material and design variables, this program was temporarily suspended, and conventional heat transfer calculations were used.

Heat transfer calculations were based on temperature data reduced from a firing made with a pressed and sintered plain tungsten insert. These data were obtained with two $\frac{1}{8}$-in.-diam tungsten/tungsten plus 26% rhenium thermocouples that were placed in the nozzle insert. One platinum/platinum plus 13% rhodium thermocouple was placed in contact with the outer diameter of the insert. Fig. 7 shows their locations.

Data taken at 15.5 sec (near steady-state conditions) were as follows:

Thermocouple	5	6	1
Temperature, °F	4200	3860	3155

Using a thermal conductivity value of 0.002175 Btu/in.²/in./sec/°F for pressed and sintered tungsten, the heat transfer rate was calculated to be 5.4 Btu/in.²/sec. The hot-wall temperature was then calculated to be 4616°F with a temperature drop of 1284°F from a calculated gas temperature of 5900°F. The gas boundary layer transfer coefficient was calculated to be 0.00419 Btu/in.²/sec/°F. The motor chamber pressure was 585 psi at the time the data were obtained. The heat transfer coefficient, extrapolated to the design pressure of 1000 psi and 100% of the theoretical propellant performance, changes the boundary coefficient to 0.00631 Btu/in.²/sec/°F.

Laboratory Tests With Plasma Arc

The preliminary results, obtained with infiltrated tungsten, prompted the initiation of a laboratory program to test the concept of molten-metal transpiration cooling and to determine the material and design variables. Samples of graphite and tungsten of various particle size and density were infiltrated with materials selected on the basis of their heats of vaporization and boiling points (Table 2). The samples were fabricated in the shape of a cork and instrumented with thermocouples for thermal analysis. An internally tapered steel fixture, insulated with a graphite sleeve, supported the specimen and insured positive seating when high pressure gas was introduced (Fig. 11). A copper continuous-water-flow calorimeter was used to monitor the heat flux before each test (Fig. 12). The calorimeter and test fixture were mounted in a fixed position so that specimen and calorimeter faces were at equal heights. A plasma-arc heat source was mounted on a vertically adjustable arm, which was swung horizontally under specimen or calorimeter (Fig. 13). Each test began with the gun directly under the calorimeter while the arc was adjusted. After controls were set to provide the proper heat flux (15 Btu/in.²/sec, as seen by the calorimeter), the gun was moved under the specimen for a timed interval. After specimen exposure, the gun was repositioned under the

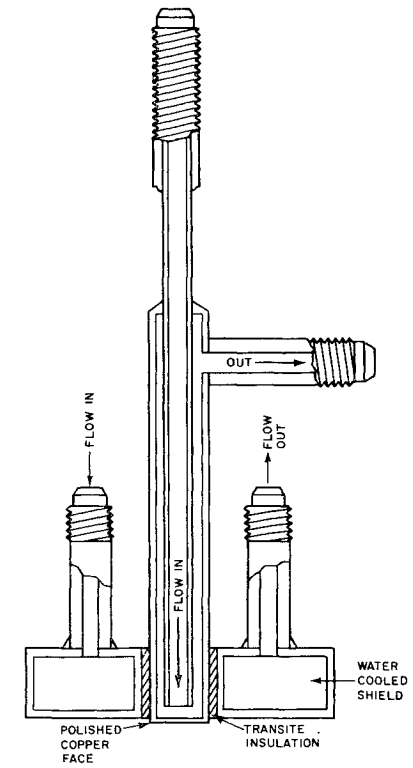

Fig. 12 Continuous water flow copper calorimeter

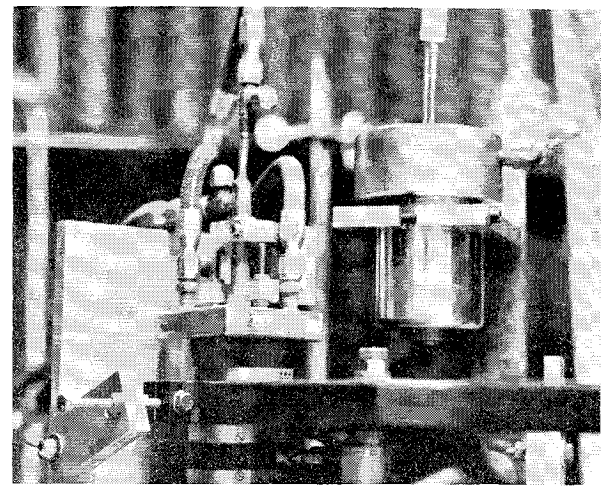

Fig. 13 Plasma-jet test facility (official U. S. Navy photograph)

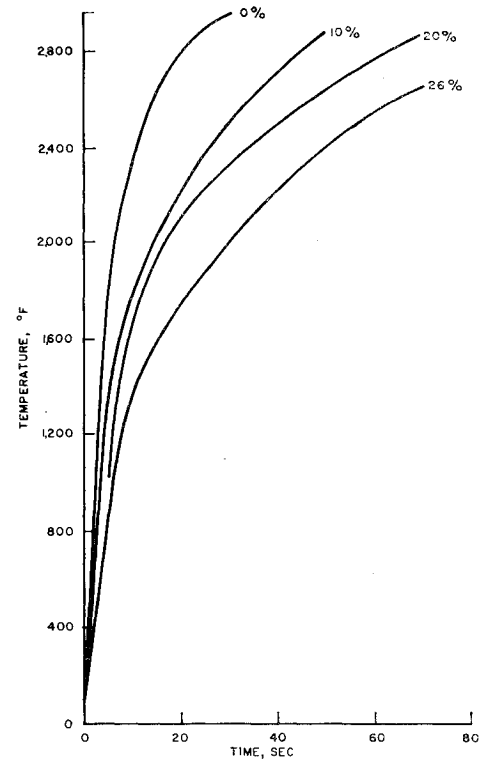

Fig. 14 Effect of weight percent copper on temperature at $\frac{1}{4}$ in. from hot wall

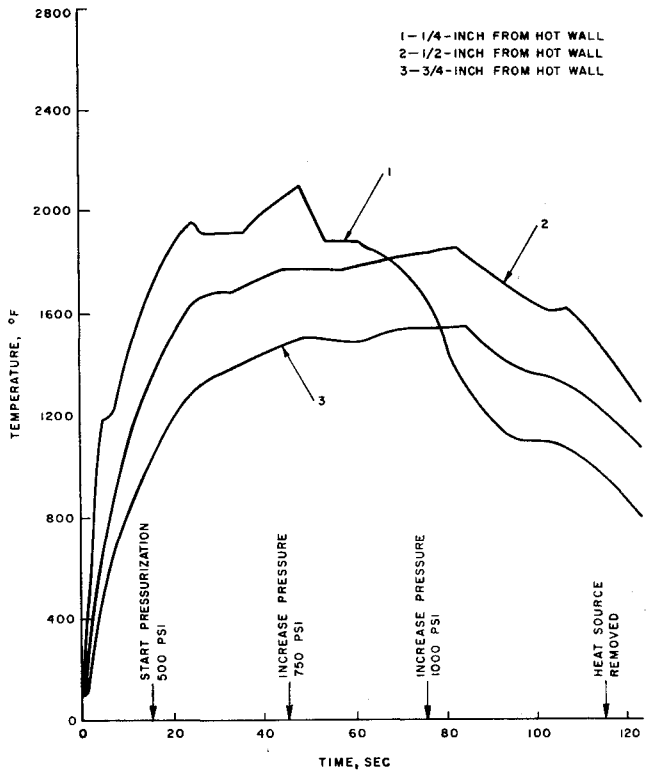

Fig. 15 Effect of pressure on time-temperature history of heated tungsten specimen containing 32 wt % copper (official U. S. Navy photograph)

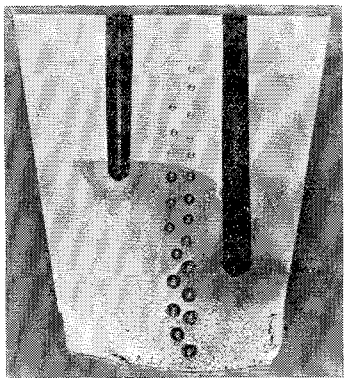

Fig. 16 Cross section of pressure plasma-arc test sample

calorimeter for a check of the heat flux. The flame impinged directly on the surface of the specimen during the test, and the temperatures at several locations in the specimen were recorded on a CEC oscillograph. Heat flux to the calorimeter was determined by mass water flow and the differential temperature of the cooling water.

Experimental Results

The first tests were performed on a series of pressed and sintered tungsten specimens containing different percentages of infiltrated copper. Fig. 14 shows the time-temperature histories taken by thermocouples placed $\frac{1}{4}$ in. from the hot surface. A comparison of these curves shows that, by increasing the percentage of copper up to 26 wt %, the temperature $\frac{1}{4}$ in. from the heated surface decreases. Furthermore, the increased percentages of copper were helpful in preserving the surface during exposure. Metallographic examination of both test specimens and the copper-infiltrated tungsten nozzle inserts after exposure revealed that only relatively small amounts of copper were depleted near the surface, and the major portion of the infiltrant remained in place. The results were encouraging but did not disclose whether surface cooling was taking place from mass transfer of copper to the boundary or whether cooling was resulting from the sensible and latent heat of fusion of copper. It was decided that, if transpiration cooling was occurring, the principle could be made more efficient by effecting continuous flow of copper to the surface. This was accomplished by pressurizing the back side of specimens with argon. A test was initiated in the usual way, but after an interval of 15 sec, the specimen was subjected to 500 psi. The pressure was increased two more times (750 and 1000 psi) during the run, with concurrent drops in temperature. The time-temperature curves for this test are shown in Fig. 15.

Post-fire examination of the pressurized specimen revealed minor surface erosion at the area of flame impingement. Weight and density measurements showed that 9.5 g of copper and 0.3 g of tungsten were removed in the 2-min run. Fig. 16 illustrates a cross section of the specimen after testing.

It is believed that the drops in the time-temperature curves do not reflect the true temperatures of the specimen. This discrepancy may be due to differential thermal expansion between specimen holder and thermocouple probe causing poor thermal contact, in addition to the effect of a cooler gas finding a selective path down the thermocouple well.

The final test in this series was conducted with a copper-infiltrated tungsten specimen (90% tungsten and 10% copper by weight). Tungsten/tungsten plus 26% rhenium thermocouples were copper brazed in the wells to prevent preferential gas flow. One surface of the sample was exposed to the plasma arc for approximately 2 min while the opposite face was pressurized with 500 psi argon. Post-fire examination showed a small amount of erosion, which is typical of low-copper-content specimens. The infiltrant was depleted to a depth of $\frac{1}{16}$ in. from the hot wall, and braze metal on the back surface had been absorbed. The time-temperature curves (Fig. 17) show increasing temperature with time rather than reversals of slope obtained during the previous pressurized test (Fig. 15). The recorded temperature regime is also higher, indicating effective blocking of gas from the thermocouple wells. The time-temperature data of a similar, but unpressurized, test are also plotted on Fig. 17. The two sets of curves illustrate the increased cooling capability of a pressurized infiltrated sample as compared with an unpressurized one.

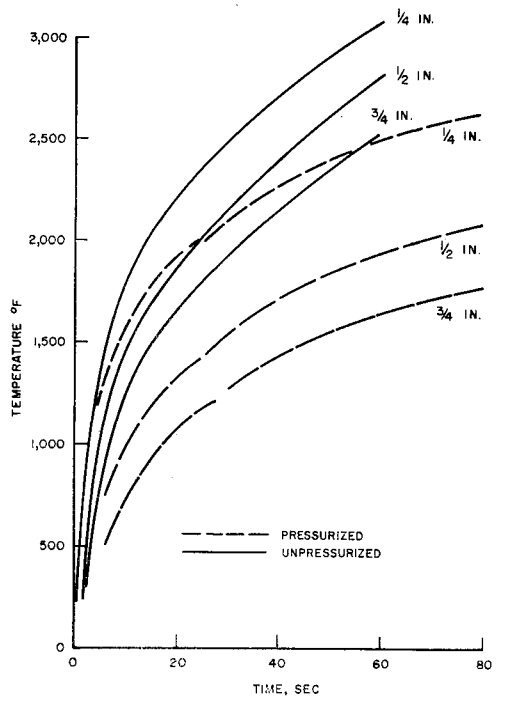

Fig. 17 Comparison of pressurized and unpressurized pressed and sintered tungsten samples containing 10 wt % copper